Journal of Power Sources 198 (2012) 423–427

Contents lists available at SciVerse ScienceDirect

Journal of Power Sources

journal homepage: www.elsevier.com/locate/jpowsour

Short communication

Supercapacitor performances of thermally reduced graphene oxide

Bing Zhao [a], Peng Liu [a], Yong Jiang [a,*], Dengyu Pan [a], Haihua Tao [b], Jinsong Song [a], Tao Fang [a], Weiwen Xu [a]

[a] School of Environmental and Chemical Engineering, Shanghai University, Shanghai 200444, PR China
[b] Shanghai Entry-Exit Inspection and Quarantine Bureau, Shanghai 200135, PR China

ARTICLE INFO

Article history:
Received 16 August 2011
Received in revised form
21 September 2011
Accepted 25 September 2011
Available online 1 October 2011

Keywords:
Pyrolysis graphene
Graphite oxide
Oxygen-containing groups
Electrical conductivity
Specific capacitance

ABSTRACT

In this paper, graphene sheets with different reduction levels have been produced through thermal reduction of graphene oxide in the temperature range of 200–900 °C. The effects of interlayer spacing, oxygen content, BET specific surface area and disorder degree on their specific capacitance were explored systematically. The variation of oxygen-containing groups was shown to be a main factor influencing the EDL capacitor performances of the pyrolytic graphene. The highest capacitance of 260.5 F g^{-1} at a charge/discharge current density of 0.4 A g^{-1} was obtained for the sample thermally reduced at about 200 °C.

1. Introduction

In order to solve environmental issues and depletion of fossil fuels, researchers have paid great attention to the development of alternative energy storage-conversion devices. Supercapacitors are such attractive devices because of their high power performances, long cycle life, wide range of operation temperature, and high rates of charge and discharge [1].

According to charge storage mechanisms, supercapacitors are classified into two types: (i) electrochemical double layer capacitors (EDLC) that store energy non-Faradically through the accumulation of charges at the electrode–electrolyte interface and (ii) redox capacitors that store energy Faradically by battery-type oxidation–reduction reactions leading to a pseudocapacitive behavior [2]. Commonly used double-layer supercapacitor electrode materials are mainly porous carbon materials (activated carbon, carbon aerogels, mesoporous carbon and carbon nanotubes, etc.) [3–6]. A new class of carbon material, graphene, has recently attracted much interest because of its unique structure and superior properties [7]. It is the flat monolayer of carbon atoms in sp^2 hybridization. This type of highly aromatic two-dimensional macromolecule with exceptionally high electrical conductivity and a high specific surface area (2630 m^2 g^{-1}) is a potential candidate as a novel electrode material for electrochemical energy storage. The intrinsic capacitance of graphene was found to be 21 μF cm^{-2} [8], the value setting the upper limit of EDL capacitance for carbon-based materials. The theoretical EDLC storage capability of monolayer graphene is estimated up to 550 F g^{-1}, provided that its entire surface area is utilized.

Graphene can be prepared on a large scale by reducing graphene oxide (GO). Some reducing methods have been developed, including chemical reduction with sodium borohydride [9] or hydrazine hydrate [10], thermal reduction [8,11,12] and electron beam reduction [13]. Compared with other reduction routes, thermal reduction can produce few layer graphene with less agglomeration, higher specific surface area, and higher electrical conductivity [14,15]. Recently, graphene sheet-based EDLC materials have been prepared by thermal reduction of GO [11,12,16] at temperature above 1000 °C. However, little has been reported on the systematical studies of the effects of calcination temperature on their specific capacitance. In this paper, different deoxygenation degrees of GO were obtained by changing thermal reduction temperature (150–900 °C). The effects of structural parameters such as interlayer spacing, oxygen content, surface area and disorder degree on specific capacitance were discussed in detail. Oxygen content in graphene was found to be a critical factor influencing the EDL capacitor performance. The specific capacitance up to 260.5 F g^{-1} was obtained in graphene reduced at about 200 °C.

2. Experiment

2.1. Synthesis of graphite oxide

GO sheets were prepared from natural graphite powder via a modified Hummers method as described in our previous work [17]. Typically, graphite powder (3 g) was put into an 80 °C solution of

* Corresponding author. Tel.: +86 21 66137508; fax: +86 21 66137508.
E-mail address: jiangyong@shu.edu.cn (Y. Jiang).

0378-7753/$ – see front matter © 2011 Elsevier B.V. All rights reserved.
doi:10.1016/j.jpowsour.2011.09.074

concentrated H_2SO_4 (12 ml), $K_2S_2O_8$ (2.5 g), and P_2O_5 (2.5 g). The mixture was kept at 80 °C for 4 h and then cooled to room temperature, diluted with deionized water (DI, 0.5 L), and left overnight. The mixture was centrifuged, washed with DI water and dried. The preoxidized graphite was further oxidized in concentrated H_2SO_4 (120 ml) and $KMnO_4$ (15 g) for 2 h under stirring and cooling conditions. Then, the mixture was diluted with DI water (250 ml) in an ice bath to keep the temperature below 50 °C for 2 h and further diluted with DI water (700 ml); 30% H_2O_2 (20 ml) was then added to the mixture and a brilliant yellow product was formed. The product was centrifuged and washed with 1:10 HCl (1 L) aqueous solution and DI water (1 L) to remove the metal ions and acid. The resulting GO sheets were dried at 150 °C in a vacuum.

2.2. Thermal reduction

GO sheets (0.2 g) were thermally reduced in a simple horizontal tube furnace in a nitrogen atmosphere with heating rate of 5 °C min^{-1}. The annealing temperature was varied from 200 to 900 °C for 2 h. The obtained samples were denoted as GNS-200, GNS-300, etc.

2.3. Characterization of graphene

X-ray powder diffraction patterns were obtained from Japan Regaku D/max-2500 using Cu Kα radiation. Fourier transform infrared (FTIR) spectra were recorded with a Bio-Rad FTIR spectrometer FTS 165. Raman spectra were recorded on Renishaw Raman microscope with a 514.5 nm laser (5 mW). Electronic conductivities were measured using a SZT-2A dc four-point probe measurement (Suzhou Tongchuang Ltd., China). The nominal radius of a probe tip was specified to be 100 μm. Equal probe spacing was 1 mm and downward force was approximately of 0.2 kg per probe.

2.4. Electrode fabrication and electrochemical measurements

The electrochemical performance of the graphene electrodes was evaluated on a CHI 660C workstation (China). Cyclic voltammogram (CV) and chronopotentiometry (CP) tests were performed in a three-electrode cell with Pt foil as the counter electrode and a saturated calomel electrode (SCE) as the reference electrode. The electrolyte was 6 M KOH. The working electrode with a thickness of 0.3 mm after pressing was fabricated by mixing 80% active materials with 20% polytetrafluoroethylene (PTFE) onto a copper mesh. Graphene nanosheet powder was pressed into tablets of 1 cm × 1 cm under a pressure of 25–30 MPa.

3. Results and discussion

Fig. 1 shows the XRD patterns of pristine GO and graphene sheets reduced at different pyrolytic temperatures. The diffraction peaks of the pristine GO appear at around $2\theta = 10°$ and 42°, corresponding to the (0 0 2) and (1 1 1) reflections of GO. The interlayer spacing calculated from the (0 0 2) reflection is 8.80 Å, far larger than that of graphite (3.34 Å). The large expansion of d_{002} is ascribed to the insertion of O-containing groups and H_2O molecules. For graphene sheets, when the pyrolytic temperature was increased from 200 to 900 °C, the (0 0 2) peak was found to shift to larger diffraction angles, corresponding to the decrease in the interlayer spacing from 3.78 to 3.37 Å (see Table 1). The intensity of the (0 0 2) peak was significantly reduced with increasing the pyrolytic temperature, especially above 500 °C. The contraction of the interlayer distance is due to the thermal removal of oxygen-containing functional groups [18]. The weakened intensity of the (0 0 2) peak indicates that the layer number of graphene sheets was gradually decreased because of the intensive thermal exfoliation of GO layers at high temperatures.

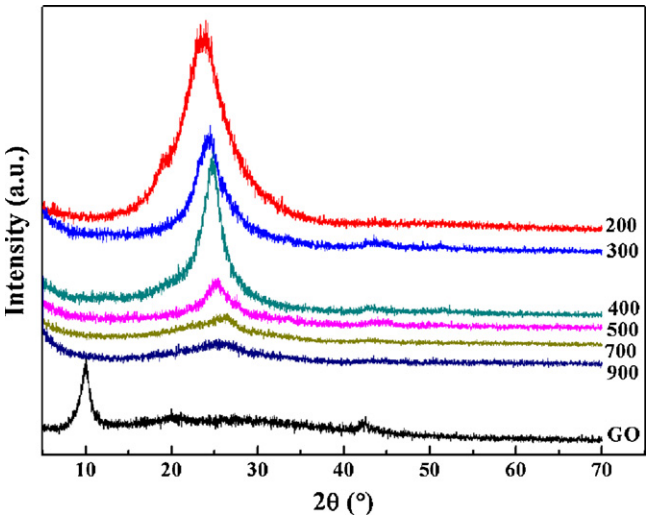

Fig. 1. XRD patterns for the pyrolytic GO for various T_{HT}.

Fig. 2 shows the FTIR spectra for the GO and graphene sheets. The pristine GO shows a C–O stretch at 1209 cm^{-1}, a O–H stretch at 3459 cm^{-1}, and a C=O stretch at 1711 cm^{-1}. With the increase in the pyrolytic temperature, the C–O and C=O stretches became almost indistinguishable, and the C=C stretching vibration at 1629 cm^{-1} increased gradually, indicating that most O-containing groups were removed by the pyrolysis through the release of H_2O and CO_2 gases. Upon pyrolysis at 900 °C, the peaks of O-containing groups almost disappeared due to their nearly complete decomposition. The EDS analysis of these samples (Table 1) shows the ratio of C/O increased with the pyrolytic temperatures, confirming the thermal decomposition of the functional groups.

Fig. 3 shows the Raman spectra of these samples, and the intensity ratios of the D to G bands (I_D/I_G) are listed in Table 1, reflecting the significant structural changes during the thermal exfoliation progress. The spectra display the carbon D and G band peaks at ~1330 cm^{-1} and 1600 cm^{-1}, respectively. The G peak corresponds to the E_{2g} phonon at the Brillouin zone center, while the D band is a breathing mode of κ-point phonons of A_{1g} symmetry. A prominent D band originating from defects such as vacancies, grain

Table 1
Structural parameters and elemental composition of the pyrolytic GO.

Sample	Interlayer spacing (Å)	EDS			I_D/I_G
		Carbon content	Oxygen content	C/O ratio	
GNS-200	3.78	79.87	21.13	3.7799	1.304
GNS-300	3.67	80.31	19.69	4.0787	1.302
GNS-400	3.59	83.82	18.18	4.6106	1.307
GNS-500	3.53	84.76	15.24	5.5617	1.212
GNS-700	3.41	89.53	10.47	8.5511	1.263
GNS-900	3.37	100	0	–	1.010

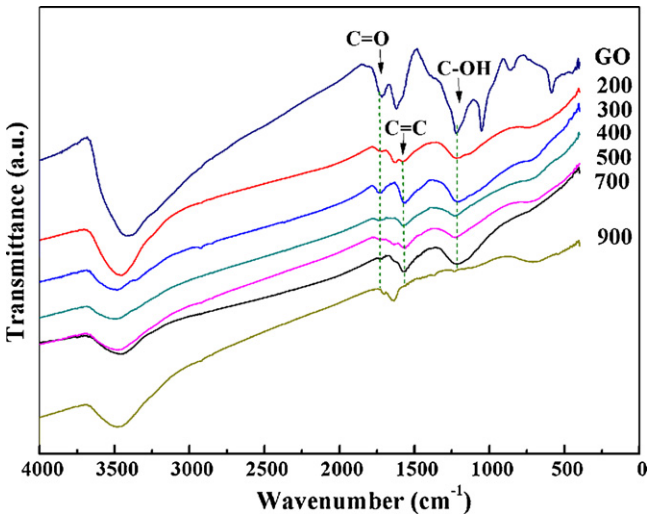

Fig. 2. FTIR spectra for the pyrolytic GO at various T_{HT}.

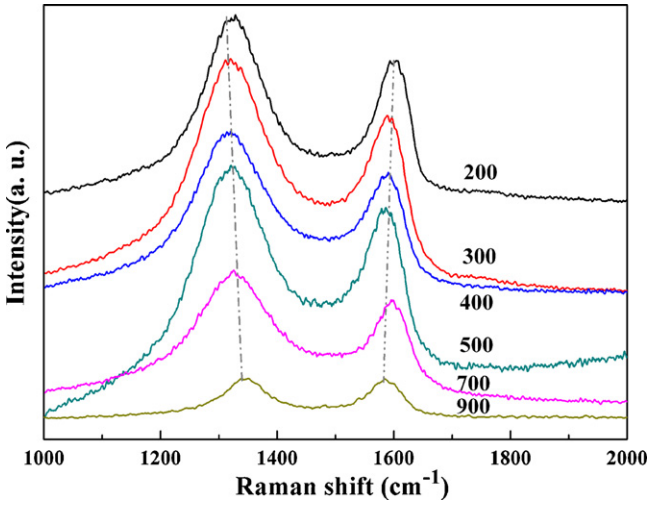

Fig. 3. Raman spectra for the pyrolytic GO at various T_{HT}.

boundaries, and amorphous carbon species is an indication of substantial disorder in the graphene sheets [10,19]. It is well documented that the I_D/I_G ratio is a measure of disorder degree and size of sp^2 clusters in a network of sp^3 and sp^2 bonded carbons [20]. The I_D/I_G ratio was found to decrease with increasing the pyrolytic temperature, indicating the decrease of disorder degree and the increase in size of sp^2 clusters. However, there is an exception in the GNS-700, whose I_D/I_G ratio is higher than that of the GNS-500. The red-shift of the G peak is about 15 cm^{-1} with raising temperature, likely because graphene has a negative coefficient of thermal expansion [21,22].

Table 2 lists the BET surface area of the graphene samples. The BET surface area increased obviously with the increase in the annealing temperature from 200 to 500 °C, because the thermal removal of the functional groups mainly occurs in this temperature range [23,24]. As the annealing temperature was further raised from 500 to 900 °C, however, the BET surface area was found to decrease from 227 to 154 $m^2\,g^{-1}$, which occurs owing to the partial overlap and coalescence of graphene sheets induced by high-temperature annealing [11]. Note that the BET surface areas of all the samples are much lower than the theoretical limit (2630 $m^2\,g^{-1}$) of graphene. The low BET values arise from the incomplete exfoliation of GO and coalescence during the thermal reduction.

The electrical conductivities of the graphene samples were measured by a dc four-probe method and the data are listed in Table 2. The electrical conductivity was found to increase slowly as the pyrolytic temperature increased from 200 to 500 °C. However, the GNS-700 and GNS-900 samples did not follow this rule, which is consistent with the abnormal change of the I_D/I_G ratio for the two samples (Table 1). Carboxyl, hydroxyl, or epoxy groups bonded on graphene and other atomic-scale lattice defects can affect the electron transport of graphene [25]. Therefore, the electrical conductivity of the low temperature pyrolytic GO samples increases gradually with the removal of the functional groups [26]. However, when graphene nanosheets are annealed at higher temperature, smaller dimensions of graphene are obtained [27] and thus interface electrical resistance increases [28].

Fig. 4 shows the discharge curves of GNS-200, GNS-400, GNS-500 and GNS-700 in 6 M KOH solution in the range of −0.95 to −0.1 V (versus SCE). The current densities are set as 0.4, 0.8, 4 and 20 $A\,g^{-1}$. The specific capacitance can be calculated by the equation $C_m = It/m\Delta V$ [29], where I is the current of charge/discharge, t is the time of discharge, ΔV is 0.85 V, and m is the mass of active materials in the working electrode. At a low discharge current (0.4 $A\,g^{-1}$), the evaluated specific capacitance of the GNS-200 is 260.5 $F\,g^{-1}$, whereas those of the GNS-500 and GNS-700 are about 105.0 and 61.7 $F\,g^{-1}$, respectively. With increasing charge/discharge current densities, the capacitance of GNS-200 decreases gradually from 200.6 $F\,g^{-1}$ (at 4 $A\,g^{-1}$) to 153.6 $F\,g^{-1}$ (at 20 $A\,g^{-1}$). The capacitance retentions in the two cases are 77.0% and 59.0%, respectively. However, the discharge capacitance of GNS-500 decreases sharply to 56.0 $F\,g^{-1}$ at a current density of 4 $A\,g^{-1}$, with only 53.3% retention.

The specific capacitance versus current density curves for all samples are shown in Fig. 5. The specific capacitance was found to decrease gradually with increasing discharge current density. Also, with increasing the annealing temperature from 200 to 900 °C, the capacitance of graphene decreases gradually. Among these samples, graphene thermally reduced at 200 °C has the highest specific capacitance. This is due to the fact that a lot of functional groups exist on the surface of the sheets of GNS-200. Hydroxyl, carboxyl, and epoxy groups are mainly attached on the external surface, which play a very important role in the charging/discharging processes, because they serve as a passage for the ions to the internal surface [3]. These functional groups were also reported to result in fast redox processes occurring at or near the electrode surface, which can provide the pseudocapacitance [16]. However, the capacitance of GNS-150 is much lower than that of GNS-200, though GNS-150 has more functional groups than GNS-200. We notice that the electrical conductivity of GNS-150 is much lower

Table 2
BET and electrical properties of the pyrolytic GO.

Sample	GNS-150	GNS-200	GNS-300	GNS-400	GNS-500	GNS-700	GNS-900
BET surface area ($m^2\,g^{-1}$)	12.25	71.50	96.78	180.71	227.05	215	154
Electrical conductivity ($s\,cm^{-1}$)	2.1×10^{-4}	3.28	13.84	14.76	17.78	7.05	9.24
Capacity ($F\,g^{-1}$)							
0.4 $A\,g^{-1}$	199.0	260.5	225.7	195.9	105.0	61.6	30.6
4 $A\,g^{-1}$	152.1	200.6	179.3	155.7	56.0	39.5	18.8

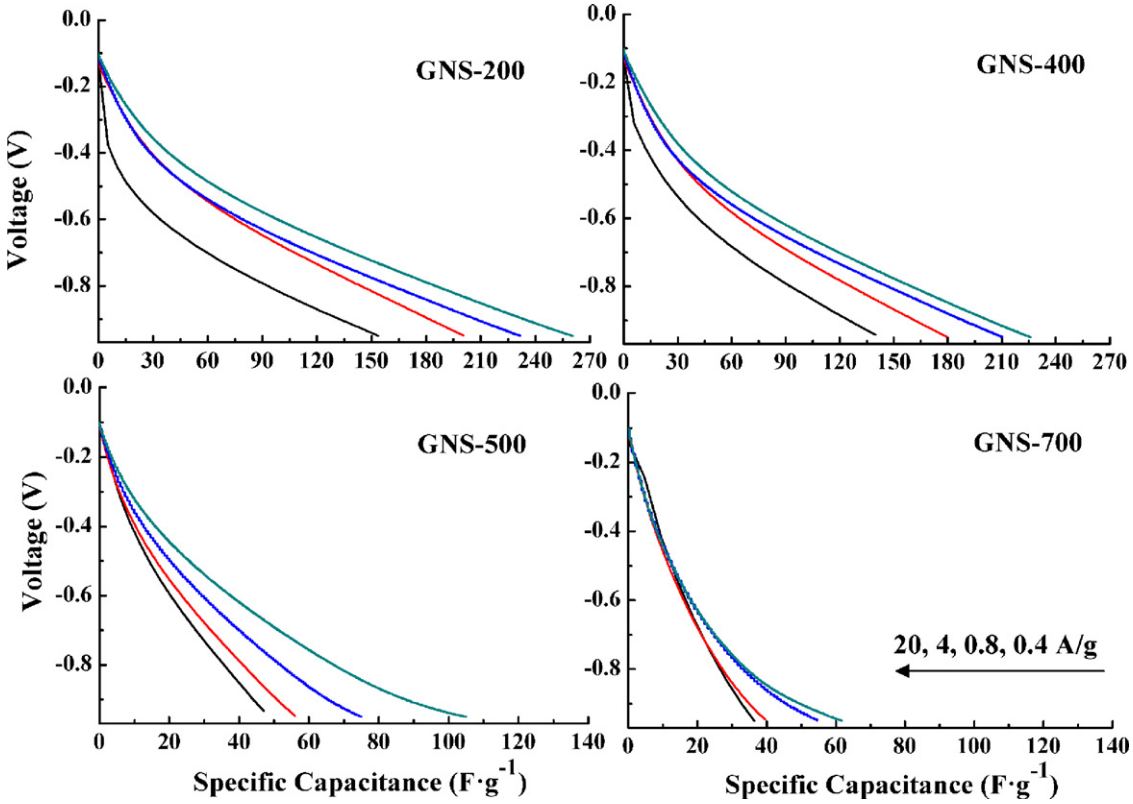

Fig. 4. Discharge curves obtained in 6 M KOH for GNS-200, GNS-400, GNS-500 and GNS-700 at different current densities.

than that of all other samples and the BET specific surface area of GNS-150 is smaller than that of GNS-200 (see Table 2). Therefore, we believe that the lower electrical conductivity (2.1×10^{-4} S cm^{-1}) and the smaller surface area (12.25 m^2 g^{-1}) may decrease the capacitance for pristine GO.

In comparison with high capacitance of graphene materials reported in other literature, there could be three aspects for the electrochemical performances of thermally reduced graphene oxide. Firstly, there are much O-containing groups and defects on the GO synthesized by Hummers method. This will decrease greatly electrical conductivity of the material. Second, the calcinations time (ca. 2 h) may be not long enough to make GO decompose completely. Moreover, we did not add conductive carbon (such as carbon black and acetylene black) to the working electrode.

The EDL specific capacitance of reduced GO was suggested to be also related to the lattice spacing of the material [30]. In our case, there is only a small difference (from 3.78 to 3.37 Å) in the d_{002} value for these tested samples. Therefore, the influence of the lattice spacing on the specific capacitance is considerably small. Relatively speaking, the sharp decrease of specific capacitance, especially for the samples prepared above 500 °C (Table 2), is much in accordance with the fast decrease of oxygen content.

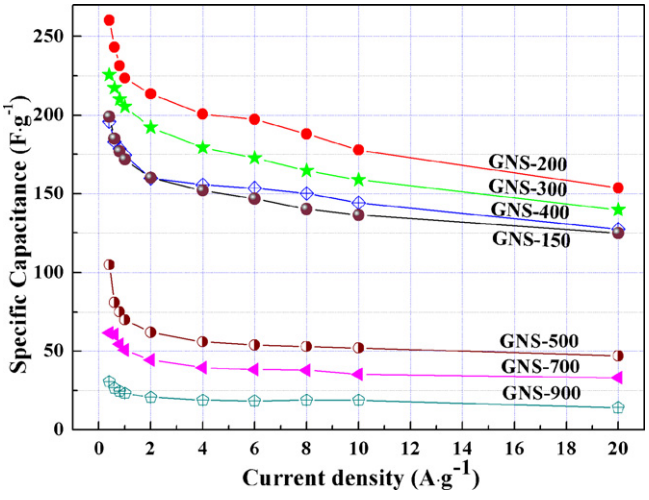

Fig. 5. Rate capacitances of the samples in 6 M KOH with different current densities.

4. Conclusions

In summary, graphene sheets with different reduction levels have been produced through thermal reduction of GO in the temperature range of 200–900 °C. The effects of interlayer spacing, oxygen content, BET specific surface area and disorder degree on their specific capacitance were explored systematically. The variation of oxygen-containing groups was shown to be a main factor influencing the EDL capacitor performances of the pyrolytic graphene. The highest capacitance of 260.5 F g^{-1} at a charge/discharge current density of 0.4 A g^{-1} was obtained for the sample thermally reduced at about 200 °C.

Acknowledgements

This work is supported by the Innovation Program of Shanghai Municipal Education Commission (10YZ03 and 10YZ05), Natural Science Foundation of Shanghai (09ZR1411800 and 10ZR1411300), Shanghai Key Laboratory of Green Chemistry and Chemical Processes (ECNU), Laboratory of Chemical Engineering (ECUST), and Shanghai Leading Academic Discipline Project (No. S30109).

References

[1] B.E. Conway, Electrochemical Supercapacitors: Scientific Fundamentals and Technological Applications, Plenum Publishers, New York, 1999.
[2] B.E. Conway, J. Electrochem. Soc. 138 (1991) 1539–1548.
[3] C.H. Kim, S.I. Pyun, H.C. Shin, J. Electrochem. Soc. 149 (2002) A93–A98.
[4] H. Probstle, C. Schmitt, J. Fricke, J. Power Sources 105 (2002) 189–194.
[5] Q.A. Li, R.R. Jiang, Y.Q. Dou, Z.X. Wu, T. Huang, D. Feng, J.P. Yang, A.S. Yu, D.Y. Zhao, Carbon 49 (2011) 1248–1257.
[6] E. Frackowiak, F. Beguin, Carbon 40 (2002) 1775–1787.
[7] K.S. Novoselov, A.K. Geim, S.V. Morozov, D. Jiang, Y. Zhang, S.V. Dubonos, I.V. Grigorieva, A.A. Firsov, Science 306 (2004) 666–669.
[8] J. Xia, F. Chen, J. Li, N. Tao, Nat. Nanotechnol. 4 (2009) 505–509.
[9] H.J. Shin, K.K. Kim, A. Benayad, S.-M. Yoon, H.K. Park, I.-S. Jung, M.H. Jin, H.-K. Jeong, J.M. Kim, J.-Y. Choi, Y.H. Lee, Adv. Funct. Mater. 19 (2009) 1987–1992.
[10] Y. Zhou, Q.L. Bao, A.L. Tang, Chem. Mater. 21 (2009) 2950–2956.
[11] M.J. McAllister, J.L. Li, D.H. Adamson, H.C. Schniepp, A.A. Abdala, J. Liu, M.H. Alonso, D.L. Milius, R. Car, R.K. Prud'homme, I.A. Aksay, Chem. Mater. 19 (2007) 4396–4404.
[12] H.C. Schniepp, J.L. Li, M.J. McAllister, H. Sai, M. Herrera-Alonso, D.H. Adamson, R.K. Prud'homme, R. Car, D.A. Saville, I.A. Aksay, J. Phys. Chem. B 110 (2006) 8535–8539.
[13] L. Chen, Z. Xu, J. Li, C. Min, L. Liu, X. Song, G. Chen, X. Meng, Mater. Lett. 65 (2011) 1229–1230.
[14] W.Z. Bao, F. Miao, Z. Chen, H. Zhang, W.Y. Jang, C. Dames, C.N. Lau 1, Nat. Nanotechnol. 4 (2009) 562–566.
[15] G. Peng, H. Song, X.H. Chen, Electrochem. Commun. 11 (2009) 1320–1324.
[16] Q. Du, M. Zheng, L. Zhang, Y. Wang, J. Chen, L. Xue, W. Dai, G. Ji, J. Cao, Electrochim. Acta 55 (2010) 3897–3903.
[17] D.Y. Pan, S. Wang, B. Zhao, M.H. Wu, H.J. Zhang, Y. Wang, Z. Jiao, Chem. Mater. 21 (2009) 3136–3142.
[18] P.C. Lian, X.F. Zhu, S.Z. Liang, Z. Li, W.S. Yang, H.H. Wang, Electrochim. Atca 55 (2010) 3909–3914.
[19] A.C. Ferrari, J. Robertson, Phys. Rev. B 61 (2000) 14095–14107.
[20] C. Navarro, R.T. Weitz, A.M. Bittner, M. Scolari, A. Mews, M. Burghard, K. Kern, Nano Letters 7 (2007) 3499–3503.
[21] I. Calizo, S. Ghosh, W.z. Bao, F. Miao, C.N. Lau, A.A. Balandin, Solid State Commun. 149 (2009) 1132–1135.
[22] T.V. Cuong, V.H. Pham, Q.T. Tran, J.S. Chung, E.W. Shin, J.S. Kim, E.J. Kim, Mater. Lett. 64 (2010) 765–767.
[23] A.B. Bourlinos, D. Gournis, D. Petridis, T. Szabo, A. Szeri, I. Dekany, Langmuir 19 (2003) 6050–6055.
[24] Z. Ji, J. Wu, X. Shen, H. Zhou, H. Xi, J. Mater. Sci. 46 (2011) 1190–1195.
[25] G.M. Rutter, J.N. Crain, N.P. Guisinger, T. Li, P.N. First, J.A. Stroscio, Science 317 (2007) 219–222.
[26] D.Y. Qu, J. Power Sources 109 (2002) 403–411.
[27] B. Zhao, G. Zhang, J. Song, Y. Jiang, H. Zhuang, P. Liu, T. Fang, Electrochim. Acta 56 (2011) 7340–7346.
[28] P.M. Ajayan, B.I. Yakobson, Nat. Mater. 10 (2011) 415–417.
[29] M.B. Zheng, J. Cao, S.T. Liao, J.S. Liu, H.Q. Chen, Y. Zhao, W.J. Dai, G.B. Ji, J.M. Cao, J. Tao, J. Phys. Chem. C 113 (2009) 3887–3894.
[30] M.M. Hantel, T. Kaspar, R. Nesper, A. Wokaun, R. Kötz, Electrochem. Commun. 13 (2011) 90–92.